Separation Science and Technology

ISSN: 0149-6395 (Print) 1520-5754 (Online) Journal homepage: www.tandfonline.com/journals/lsst20

Mass Transfer- Fluid Flow Interactions in Perforated Plate Extractive Reactors

Reem S. Ettouney, Mahmoud A. El-Rifai, Ayat O. Ghallab & Amira K. Anwar

To cite this article: Reem S. Ettouney, Mahmoud A. El-Rifai, Ayat O. Ghallab & Amira K. Anwar (2015) Mass Transfer- Fluid Flow Interactions in Perforated Plate Extractive Reactors, Separation Science and Technology, 50:12, 1794-1805, DOI: 10.1080/01496395.2015.1014057

To link to this article: https://doi.org/10.1080/01496395.2015.1014057

Separation Science and Technology, 50: 1794–1805, 2015

ISSN: 0149-6395 print / 1520-5754 online
DOI: 10.1080/01496395.2015.1014057

Taylor & Francis
Taylor & Francis Group

Mass Transfer- Fluid Flow Interactions in Perforated Plate Extractive Reactors

Reem S. Ettouney, Mahmoud A. El-Rifai, Ayat O. Ghallab, and Amira K. Anwar
Department of Chemical Engineering, Faculty of Engineering, Cairo University, Giza, Egypt

Coupling between extraction, reaction, and liquid-liquid contact hydrodynamics have quantitative as well as qualitative implications on the performance of un-agitated perforated plate extractive reactors. Models, which take into account the effect of flow dynamics on mass transfer performance, are developed to analyze the steady state behavior of such columns when conducting a chemical reaction in the continuous extract phase. New expressions are derived for the composition profiles in the cases of physical extraction, slow, and infinitely fast reactions. Typical results show that the raffinate purity may either increase or decrease on increasing the solvent rate depending on the interaction between column fluid dynamics, mass transfer, and reaction kinetics.

Keywords extractive reactions; mass transfer; modeling; perforated plate columns

INTRODUCTION

Extraction intensified by a chemical reaction is resorted to in applications covering the petroleum, petrochemicals, nuclear, and pharmaceutical industries (1). Typical examples include desulphurization of hydrocarbons by aqueous caustic solutions (2), extraction of uranyl nitrate by tributyl phosphate (3), extraction of phosphorus from waste water (4), extraction of hexavalent chromium from aqueous solutions (5), and removal of arsenic from natural gas condensate (6). Rigorous modeling of the performance of heterogeneous fluid-fluid reactors has to consider the interaction between the inter-phase transfer on one hand and the kinetics (7) and stoichiometry of the enhancing reaction on the other. The presence of an enhancing chemical reaction provides for higher selectivity (8) with respect to the solute to be removed and may enable a considerable reduction in the size of the equipment required to achieve a given purification duty.

Received 10 August 2014; accepted 28 January 2015.
Address correspondence to Reem S. Ettouney, Chemical Engineering Department, Faculty of Engineering, Cairo University, Giza, 12613, Egypt. E-mail: ettouney@thewayout.net

Figure 1 outlines the basic scheme required for the formulation of the conservation equations, constitutive relations, and boundary conditions in extractive reactors. The driving forces and resistances governing mass transfer and the effective reaction volumes within the contactor depend on flow dynamics of the two liquid phases. The hydrodynamic pattern obtained in the extractive reactor (9) affects relevant system characteristics such as dispersed phase volume fraction, slip velocity, interfacial area per unit volume of dispersed phase, and interfacial area per unit volume of the contactor. The physical properties of the handled fluids which affect the transport within the phases have also to be computed under the expected operating temperature range.

A wide variety of contacting equipment which differ considerably in the obtained fluid-fluid interaction pattern are in commercial use. Non ideal flow patterns in mixer-settlers can be modeled by a combination of arrangements involving back-mix and plug flow volumes (10) while plug flow and axial dispersion models may be used for describing spray (11) and packed (12) extractive reactors. Mixing cells with recycle (13) and forward mixing arising from drop size distribution and axial mixing of the continuous phase (14) have been considered for modeling spray, agitated, and pulsed extractors (15) which feature strong dispersed phase interactions with the turbulent continuous phase. Droplets breakage (16) and coalescence (17) result in distributed droplet population size and concentration (18). Recent dynamic models (19) rely on simultaneous application of computational fluid dynamics and population balance equations (1, 20). Owing to the relative complexity of such models, reduced order models have been suggested for process control studies of agitated columns (21).

Un-agitated perforated plate liquid-liquid extraction columns (22) are particularly efficient for their high liquid handling capacity and for providing good separation efficiency especially for systems with low interfacial tension which are easily dispersed and do not require mechanical agitation. Reliable empirical correlations (23) are available for describing the hydrodynamic performance of these columns and have been used to validate a computational fluid dynamic model (24).

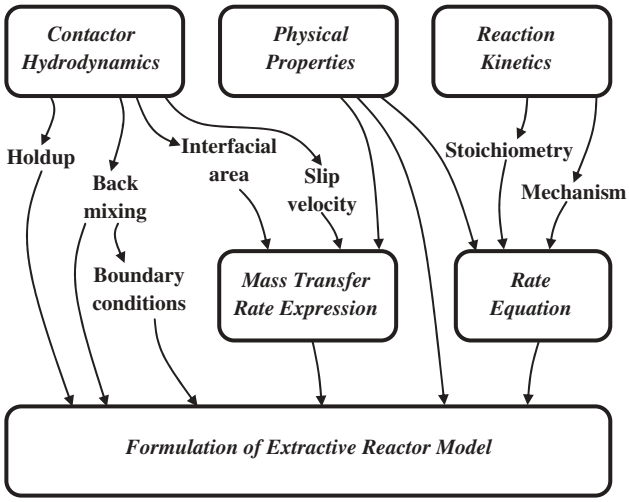

FIG. 1. Model development scheme.

Such correlations have been also integrated in models of un-agitated perforated plate extractors conducting dispersed phase reactions (25), and used to study the composition dynamics (26) and flow transients (27) in such columns. The developed models have been also simplified to reduced order linearized models.

The purpose of the present paper is to elucidate the effect of interaction between fluid flow, mass transfer, and chemical reaction on the performance of un-agitated perforated plate extractive reactors. The cases of physical extraction, a slow first order reaction in the continuous extract phase, and a very fast reaction at the interface are to be considered. Simple analytical equations derived from first principles are developed to model the system performance. The dependence of the parameters characterizing the column behavior on phase flow rates are generated on the basis of existing hydrodynamics and mass transfer coefficient correlations. A comparison of the distribution of the driving force along the column is undertaken to address the effect of phase flow rates on the concentration profiles of the extract and raffinate products in the above three cases.

THE MODEL SYSTEM

The mechanism of enhancing mass transfer through a simultaneous extract phase chemical reaction $A + f\,B \rightarrow D$ involves either lowering the mass transfer resistance and/or increasing the driving force. A comprehensive analysis of the mechanism of interaction between the rates of mass transfer and chemical kinetics (28, 29) enables identification of different regimes. The different regimes correspond to different aspects of the concentration profiles in the two film representation of inter-phase transfer between a raffinate donor phase and a sink extract phase. Figure 2 depicts four possible regimes for the mass transfer-kinetics interaction. In Fig. 2a, the solute A is extracted from the dispersed organic phase into a continuous aqueous phase where it undergoes a slow reaction with an excess of reactant B present in the aqueous phase. The A concentration profile is akin to the case of purely physical extraction; however, the interfacial solute concentration y_i and its concentration in the bulk of the extract phase x are lower than in the case of physical extraction. This corresponds to an increase of the driving force. It is obvious that the faster the reaction, the higher the improvement of the driving force. If the reaction is instantaneous, maximum enhancement occurs when the reaction takes place at the interface. This condition occurs when the rate of mass transfer of B to the interface is sufficient to react with the available reactant A, that is, the rate of transfer of B in the extract phase should be f times the rate of transfer of A to the interface in the raffinate phase. Figure 2b depicts the solute and extract phase reactant profiles for this case, the driving force in the raffinate phase is increased and the continuous extract phase resistance for solute A is eliminated. Two other intermediate cases are shown in Fig. 2c and Fig. 2d. Figure 2c depicts the profile in the case of an instantaneous reaction when the rate of mass transfer of reactant B to the interface is relatively slow. This condition occurs when the bulk concentration of B is relatively small. In this case the

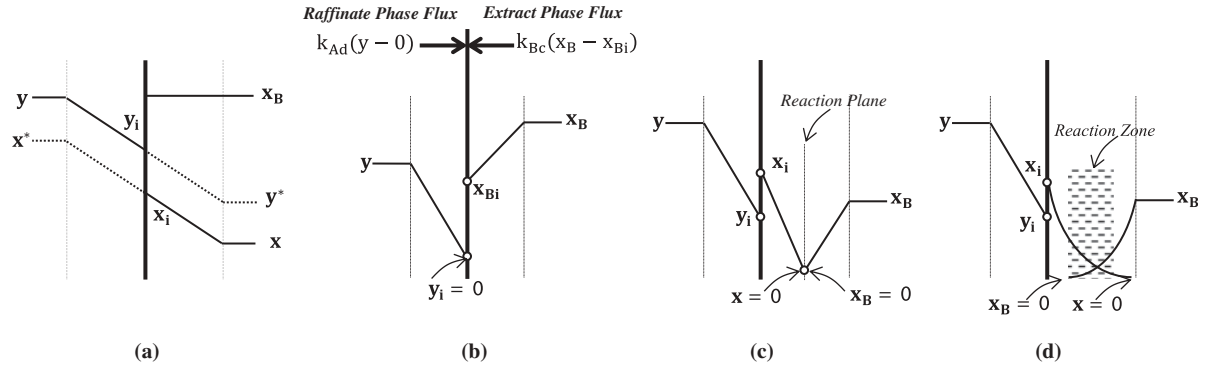

FIG. 2. Two film representation of concentration profiles, (a) slow reaction in extract phase, (b) infinitely fast reaction at interface (c) infinitely fast reaction in extract film, (d) moderately fast reaction in extract film.

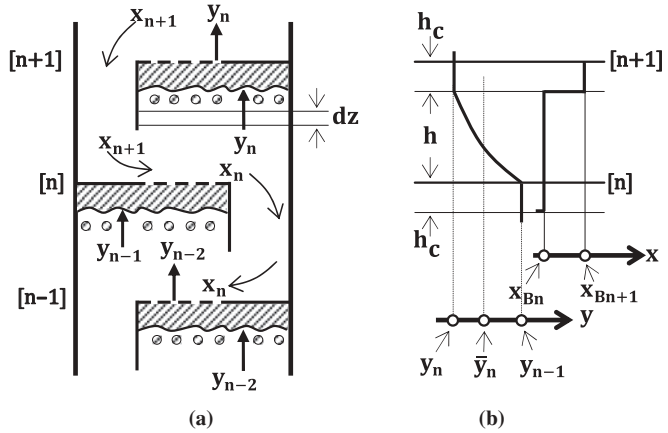

FIG. 3. (a) nomenclature of extract x and raffinate y stream compositions; (b) concentration profiles of A in raffinate and B in extract within a plate.

reaction plane lies within the extract film where the concentration of both A and B vanish. When the reaction is moderately fast both reactants A and B can co-exist in a reaction zone rather than a reaction plane. Figure 2d illustrates this situation. The models developed in the following sections are based on the cases shown in Fig. 2a for a slow extract phase reaction and Fig. 2b for an infinitely fast interfacial reaction.

Figure 3a outlines the nomenclature of the stream compositions in a perforated plate extractive reaction column. The dispersed feed phase, containing solute A, is in plug flow in the contact height above a plate while the solvent phase containing excess reactant B, which is insoluble in the raffinate feed phase, is completely mixed on each plate. The concentration of the dispersed phase does not change in the coalesced layer and that of the continuous phase also remains unchanged along the downspout. Figure 3b presents a qualitative visualization of the concentration profiles of A in the dispersed phase and of B in the continuous phase within a plate.

Slow Reaction in Extract Phase

Assuming a reasonable degree of mobility and internal circulation within the droplets, the drop mass transfer resistance may be assumed to be lumped in an internal convective film. In this case, the two film representation of the mass transfer driving forces corresponds to the diagram of Fig. 2a.

A steady state mass balance on solute A transferred from the dispersed phase drops in an increment of height dz above plate n gives

$$Vy - K_A a' \varphi A_a \left(y - y^*\right) dz = V(y + dy) \tag{1}$$

If the distribution of A between the two phases follows a linear equilibrium relation, then

$$y^* = mx \tag{2}$$

Considering a plate n, combination of Eqs. (1) and (2) gives

$$\frac{dy}{y - mx_n} = -\frac{\beta}{h} dz \tag{3}$$

which integrates between y_{n-1} and y_n to

$$x_n = \frac{y_n - \alpha y_{n-1}}{m(1 - \alpha)} \tag{4}$$

Assuming the reaction in the extract phase to follow first order kinetics with respect to A, the overall mass balance on solute A in the active plate volume gives

$$Lx_{n+1} + Vy_{n-1} = Lx_n + Vy_n + (1 - \varphi) A_a h k \, x_n \tag{5}$$

The combination of Eqs. (1) to (5) gives

$$y_{n+1} - by_n + cy_{n-1} = 0 \tag{6}$$

The boundary conditions at the feed and at the solute free solvent ends are respectively given by

$$y_o = y_f \tag{7}$$

$$x_{N+1} = 0 \tag{8}$$

The solution of the second order difference Eq. (6) subject to boundary conditions (7) and (8) enables to obtain the ratio between the raffinate concentration leaving any plate, n, and the feed concentration as

$$\frac{y_n}{y_f} = c^n \frac{a_1^{N-n}(a_1 - \alpha) - a_2^{N-n}(a_2 - \alpha)}{a_1^N (a_1 - \alpha) - a_2^N (a_2 - \alpha)} \tag{9}$$

$$\frac{x_n}{y_f} = \frac{1}{m(1 - \alpha)} \frac{c^{n-1}(a_1 - \alpha)(a_2 - \alpha)\left(a_1^{N-n+1} - a_2^{N-n+1}\right)}{a_1^N (a_1 - \alpha) - a_2^N (a_2 - \alpha)} \tag{10}$$

The concentration profile of B in the extract phase may be obtained by a mass balance on reactant B on plate n to give

$$L(x_{Bn+1} - x_{Bn}) = f(1 - \varphi) A_a h k \, x_n \tag{11}$$

$$x_{Bn} = x_{Bn+1} - f\delta x_n \tag{12}$$

The concentration of B in the bottom extract effluent may be obtained by an overall balance to give

$$x_{B1} = x_{BN+1} - f \frac{(y_o - y_N)V - Lx_1}{L} \tag{13}$$

Physical Extraction

For the special case of physical extraction, $k = 0$, $\delta = 0$, a simpler form of the analytical solution of the above system of equations is possible. This gives the concentrations of solute A leaving different plates as

$$\frac{y_n}{y_f} = 1 - \frac{(\alpha - 1)(1 - c^n)}{c^{N+1} - \alpha c^N + \alpha - 1} \tag{14}$$

$$\frac{x_n}{y_f} = \frac{1}{m}\frac{(c - \alpha)(c^N - c^{n-1})}{c^{N+1} - \alpha c^N + \alpha - 1} \tag{15}$$

Infinitely Fast Reactions

As mentioned above, maximum intensification is obtainable when the reaction between A and B takes place at the interface. If the reaction $A + f\,B \rightarrow D$ is very fast, the reaction will take place and remain at the interface when the ratio of the molar concentrations of the reactants in their respective phases is greater or equal to the inverse ratio of their mass transfer coefficients multiplied by the stoichiometric reaction factor (29). This condition will be satisfied in all plates when

$$x_{B1}/y_f \geq f(k_A/k_B) \tag{16}$$

where k_A is the dispersed phase mass transfer coefficient for solute A and k_B is the continuous phase mass transfer coefficient for reactant B.

In this case, the two film representation of the concentration gradients at any one level within the active contact height on any plate may be represented as shown in Fig. 2b. Since reactant A is immediately consumed as it reacts with reactant B at the interface, $y_i = 0$, and a simplified form of Eq. (1) is obtained

$$V\,dy = -k_A a' \varphi A_a y\,dz \tag{17}$$

which integrates to

$$y_n = e^{-\beta'} y_{n-1} = \alpha' y_{n-1} \tag{18}$$

The terminal raffinate composition reduces to

$$(y_N/y_f) = \alpha'^N \tag{19}$$

For the above reaction stoichiometry, the rates of transfer of A and B are related by

$$k_B a' \varphi A_a h\left(x_{Bn} - x_{Bi}\right) = f k_A \bar{y}_n a' \varphi A_a h \tag{20}$$

$\bar{y}_n$ may be deduced from Eqs. (17) and (18) as

$$\bar{y}_n = \frac{1}{h}\int_0^h y\,dz = \frac{(e^{\beta'} - 1)}{\beta'} y_n \tag{21}$$

The concentration of B on two successive plates may be related by overall and continuous phase balances on a plate, this gives

$$x_{Bn} = x_{Bn+1} - \frac{fV}{L}\left(\frac{1}{\alpha'} - 1\right) y_n \tag{22}$$

The concentration of B in the final extract bottom product reduces to

$$x_{B1} = x_{BN+1} - y_f \frac{fV}{L}\left(1 - \alpha'^N\right) \tag{23}$$

ESTIMATION OF MODEL PARAMETERS

It is clear from the above that the three dimensionless model parameters b, c, and α determine the static characteristics of perforated plate columns conducting a chemical reaction in the continuous extract phase. The parameters b and c are combinations of the dimensionless parameters α, δ, and g which are functions of the system physical properties, column design dimensions, and the phase flow rates. These are summarized in Table 1.

The values of the hydrodynamic and mass transfer parameters figuring in the above definitions in Table 1 have been obtained from available and comprehensively compiled correlations in the literature (23, 30, 31). A summary of the used hydrodynamic correlations is given in Table 2. For an existing column the allowable range within which the flow rates of the two phases may be varied is constrained by the hydrodynamic stability and the mass transfer surface area. The hydrodynamic stability range of phase flow rates is determined by the perforated plate column design dimensions. The maximum continuous phase downspout velocity should be smaller than the terminal falling velocity of the fine 0.6-0.8 mm droplets to avoid flooding, that is, entrainment of dispersed phase droplets to the plate below through the downspout. The depth of the coalesced layer which is the sum of the head losses of both phases should not extend beyond the length of the downspout lest the dispersed phase liquid should flow up the downspout to

TABLE 1
Model dimensionless parameters

Symbol	Definition	Symbol	Definition
α	$e^{-\beta}$	δ	$(1-\varphi)A_a hk/L$
α'	$e^{-\beta'}$	b	$1+\alpha+(1-\alpha)g+\delta$
β	$K_A a' A_a \varphi h/V$	c	$(1-\alpha)g+\alpha+\alpha\delta$
β	$k_A a' A_a \varphi h/V$	$a_{1,2}$	$(b \pm \sqrt{b^2-4c})/2$

TABLE 2
Used hydrodynamic correlations

Parameter	Correlation	Reference	Definitions in correlations
Drop diameter, d_p	$d_p = F(v_o^2, \rho_D, \Delta\rho, \sigma, d_o, \mu_C)$	Chart in [23] and [32]	v_o: Perforations velocity = V/A_p A_p: Perforations area d_o: Perforation's diameter
Holdup, φ	$v_s(1-\varphi) = F(\mu_C, \rho_C, \Delta\rho, d_p)$	Chart in [23] and [33]	v_n: net velocity = $V/(A_T - A_d)$
Slip velocity, v_s	$v_s\varphi = v_n$		A_T: Tower cross section A_d: downspout cross section
a'	$6\varphi/d_p$		
Dispersed phase pressure drop, h_D	$h_D = \frac{(v_o^2 - v_n^2)\rho_D}{2g(0.67^2\Delta\rho)} + \frac{6\sigma g_c}{d_{ps}\Delta\rho g}$	[23] and [34]	d_{ps}: drop diameters at v_o = 0.03m/s
Continuous phase pressure drop, h_C	$h_C = \frac{(4.5v_d^2)\rho_C}{2g\Delta\rho} + \frac{(v_R^2 - v_d^2)\rho_C}{2g(0.67^2\Delta\rho)}$		v_d: downspout velocity = L/A_d v_R: Restriction velocity = L/A_R A_R: downspout cross section
Depth of coalesced layer, h_c	$h_c = (h_D + h_C)$		Mass transfer height, $h = (S - h_c)$

the plate above. Another constraint on the dispersed phase flow rate is that the perforation velocity v_o should lie between 0.1 and 0.15 m s^{-1} in order to ensure uniformity of the drop size and maximization of interfacial surface.

The safe operating range of flow rates is narrower than that called for by hydrodynamic stability. Owing to possible small deviations in plate horizontality in large diameter columns, the depth of the coalesced layer, h_c should not be less than about 0.05 m to avoid mal-distribution of flow through all perforations. A restriction of smaller area, A_R, is introduced in the downspout to increase the continuous phase pressure drop at low flow rates to ensure that the low h_c constraint is not violated. On the other hand, it should not exceed about 0.15 m to avoid encroachment on the effective mass transfer height, h.

Correlations for estimation of the dispersed and continuous phase mass transfer coefficients are reported in the literature for three different droplet flow patterns namely quasi-rigid, circulating, and oscillating droplets. These correlations are reported for the dispersed and continuous phase mass transfer coefficients in Table 3. The numerical values of the coefficients used in the model calculations were taken as the arithmetic average of the predictions of the correlations for the three flow patterns. The diffusion coefficients were calculated from Wilke-Lee (40) and Hayduk and Laudie (41) correlations. The values of the physico-chemical parameters used in the above hydrodynamic and mass transfer correlations are given in Table 4. The above correlations have been applied to a 0.96 m internal diameter column containing 25 plates. The numerical values of the design parameters used with the above correlations are given in Table 5.

Since the application of the hydrodynamic correlations is rather laborious and involves iterative calculations, MatLab programs have been developed for the repetitive

TABLE 3
Mass transfer correlations

Mass Transfer Coefficient	Correlation	Reference	Remarks
Inside droplets	$k_A = 0.083d/t_e + 6.58D_d/d$	(35)	Viscous quasi rigid droplets
	$k_A = 0.079d/t_e + 17.66D_d/d$	(36)	Droplet inner circulation
	$k_A = 0.00375 + u/(1 + (\mu_D/\mu_C))$	(37)	Oscillating droplet
Outside droplets	$k_A = \frac{D_C}{d}\left(2 + 0.67\sqrt{Re_p.Sc}\right)$	(38)	Viscous quasi rigid droplets
	$k_A = \frac{D_C}{d}\left(0.6\sqrt{Re_p.Sc}\right)$	(36)	Droplet inner circulation
	$k_A = 1.2D_C^{0.5}\left(\frac{48\sigma}{\pi^2 d^3(2\rho_C + 3\rho_D)}\right)^{0.25}$	(39)	Oscillating droplet

TABLE 4
Numerical values of physico-chemical parameters

Physical property	Dispersed phase benzene containing HCl	Continuous phase aqueous NaOH
Density, kg m^{-3}	877	1000
Viscosity, kg m^{-1} s^{-1}	0.0006	0.001
Surface tension, N m^{-1}	0.03	0.07
Interfacial tension, N m^{-1}	0.04	
Diffusivity of HCl in benzene, cm^2 s^{-1}	4.21×10^{-5}	—
Diffusivity of NaOH in water, cm^2 s^{-1}	—	1.1×10^{-5}
Reaction rate constant, s^{-1}	—	0.0015

TABLE 5
Plate design parameters

Parameter	Value	Parameter	Value
A_T, m^2	0.7286	d_o, m	0.006
A_a, m^2	0.4649	*Pitch, m*	0.015
A_n, m^2	0.6083	*S, m*	0.5
A_d, m^2	0.1202	Perf. /plate	2386
A_R, m^2	0.0157	A_p, m^2	0.0675

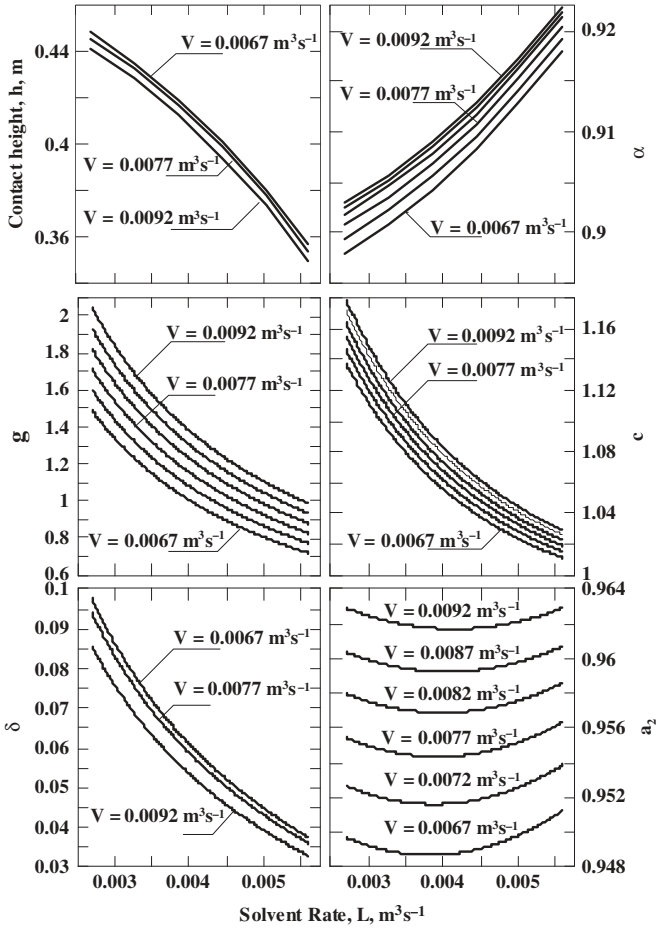

FIG. 4. Effect of continuous and dispersed phase flow rates on relevant performance parameters of an extractive reaction column.

computation of the relevant system characteristic parameters for the studied range of phase flow rates. Data available in chart form have been converted to equations to enable their use in the programs.

The developed programs have been used to generate the effects of changing the phase flow rates, within the stable column operating range. Figure 4 presents the typical outputs for the contact height, h, and the dimensionless parameters g, δ, α, c, and a_2 based on the numerical values of the physico-chemical and column design parameters reported in Tables 4 and 5, respectively. For systems involving different values of the above parameters, different numerical values would be obtained for the dimensionless quantities but the trends of variation of all the above quantities are expected to be the same.

The results show that on increasing the dispersed phase flow rate, the drop diameter and holdup increase while the slip velocity and interfacial area per unit volume decrease. This is also reflected as a reduction in the individual and overall volumetric film mass transfer coefficients. Increase in either of the phase flow rates corresponds to an increase of the height of the coalesced layer beneath a plate which means a decrease of the effective mass transfer height.

MODEL RESULTS

The steady state behavior of a column with a given number of plates may be studied by integrating the computations of the dimensionless parameters b, c, and g at different phase flow rates together with the application of the model equations pertaining to the prevailing reaction kinetic regime. In this section, a 25 plate neutralization column where a solute acid at a concentration of 0.024 kmole m^{-3} is removed from the dispersed organic phase by contact with an aqueous phase containing 0.25 kmole m^{-3} of an alkali reagent is considered. The three cases of physical extraction, slow extract phase reaction, and very fast interfacial reaction are investigated for a range of phase flow rates lying between the limits of hydrodynamic stability.

Concentration Profiles

The extract and raffinate composition profiles for the studied column are presented in Fig. 5. It is clear that the presence of a chemical reaction enhances the purification of the raffinate phase giving rise to smaller values of y_n throughout the column, maximum enhancement being obtained for the case of the very fast reaction (curve III) as shown in Fig. 5a. The concentration profile of A (x_n) in the extract is shown in Fig. 5b. Curve I corresponding to physical extraction is higher than curve II pertaining to the case of a slow reaction, while solute A in the extract phase is completely transformed into product D and does not appear in the extract phase in the case of the infinitely fast reaction. Figure 5c shows that the concentrations of reactant B in the extract phase, in the case of very fast reaction (curve III), are lower than those pertaining to the slow reaction. Reactant B is not present in the case of physical extraction.

Mass Transfer Driving Force

The distribution of the mass transfer driving force along the column may be derived by considering the mean mass transfer driving force on each plate which may be expressed in raffinate concentration units as

$$\text{Driving Force} = \bar{y}_n - mx_n \tag{24}$$

where $\bar{y}_n$ is the mean raffinate composition in the active plate height. In the cases of physical extraction and slow reaction,

$$\bar{y}_n = \frac{1}{h}\int_0^h y\,dz = -\frac{1}{\beta}\int_{y_{n-1}}^{y_n}\frac{y\,dy}{y - m\,x_n} \tag{25}$$

$$\bar{y}_n = \frac{1}{\beta}\left[(y_{n-1} - y_n) + mx_n ln\frac{y_{n-1} - mx_n}{y_n - mx_n}\right] \tag{26}$$

In the case of infinitely fast reaction, $x_n = 0$ and $\bar{y}_n$ is given by Eq. (21).

Figure 6 depicts the distribution of the mass transfer driving force along the column. It is seen that the plate concentration driving forces decrease from the bottom to the top of the column in the cases of fast and slow reactions while they increase slightly in the case of physical extraction. The average driving force along the column in solute A concentration units for the three studied cases of physical extraction, slow reaction, and instantaneous reaction are respectively 0.0068, 0.0077, and 0.0095 kmoles.m^{-3}. It is recalled that the presence of a chemical reaction reduces mass transfer resistance. In the case of infinitely fast reaction (curve III), the resistance in the extract phase is eliminated. In this case, the decrease in the driving force as we move up the column is equivalent to the decrease of the raffinate concentration. In the case of physical extraction (curve I), the driving force is higher in the upper plates where the solvent is still lean (mx_n is small in Eq. 24) and the concentration driving force drops as we move down the column. For relatively slow chemical reactions (curve II), the trend of the drop in the driving force as we move up the column observed for the fast reaction is still maintained but to a lesser extent. As the reaction rate constant decreases, the driving force profile approaches that of physical extraction.

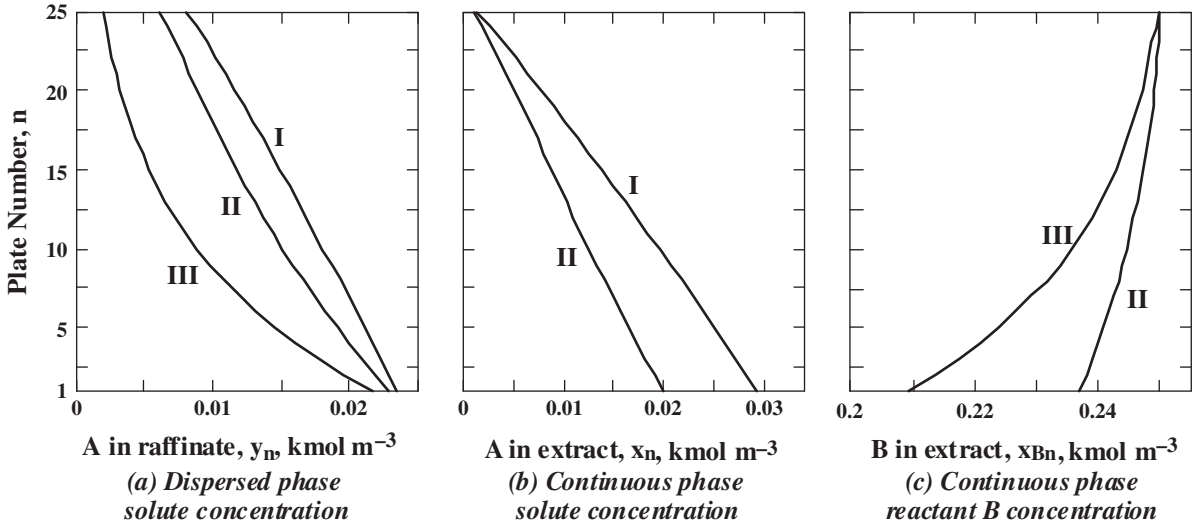

FIG. 5. Profiles of a 25 plate column, (I) physical extraction, m=0.6 (II) slow reaction, m = 0.6, k = 0.0015s^{-1} (III) fast interfacial reaction.

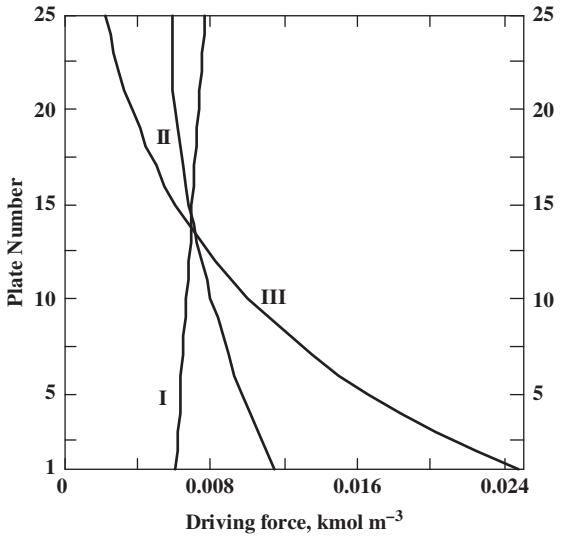

FIG. 6. Distribution of mass transfer driving force along the column.

Effect of Phase Flow Rates

Consideration of the effect of interaction between the flow conditions and the mass transfer conditions in extractive reactors is important at the phases of preliminary design of the column and anticipation of the expected range of fluctuations in operating flow rates and compositions of the contacted liquids. It is also important for the study of column control and the scheme of counteracting disturbances in feed flow rate or composition by manipulation of the phase flow rates in order to ensure that the allowable maximum and minimum phase flow rates are not surpassed for the column under consideration.

The effects of changing the feed and solvent flow rates, within the safe operating window of the studied column, on the terminal stream concentrations are depicted in Figs. 7, 8, and 9 for the cases of physical extraction, instantaneous interfacial reaction, and slow extract phase reaction, respectively. It is seen that the raffinate stream composition in all of the above cases increases as the feed flow rate is increased, that is, the higher the feed rate V, the higher the curves giving the raffinate product concentration y_{25} versus L in all cases. Also, the final extract compositions x_1 in the cases of physical extraction and slow reaction, increase as the feed rate increases and decrease as the solvent rate is increased. The above two trends are expected since they are common to counter current separation processes in general. In the case of instantaneous reactions, the solute is not present in the extract and the composition of reactant B in the extract increases with the solvent rate and decreases with the feed rate, which is also expected. In any case, increased solubility or presence of an enhancing reaction results in improved purification, that is, lower raffinate concentrations. The observed trends of raffinate composition change with solvent

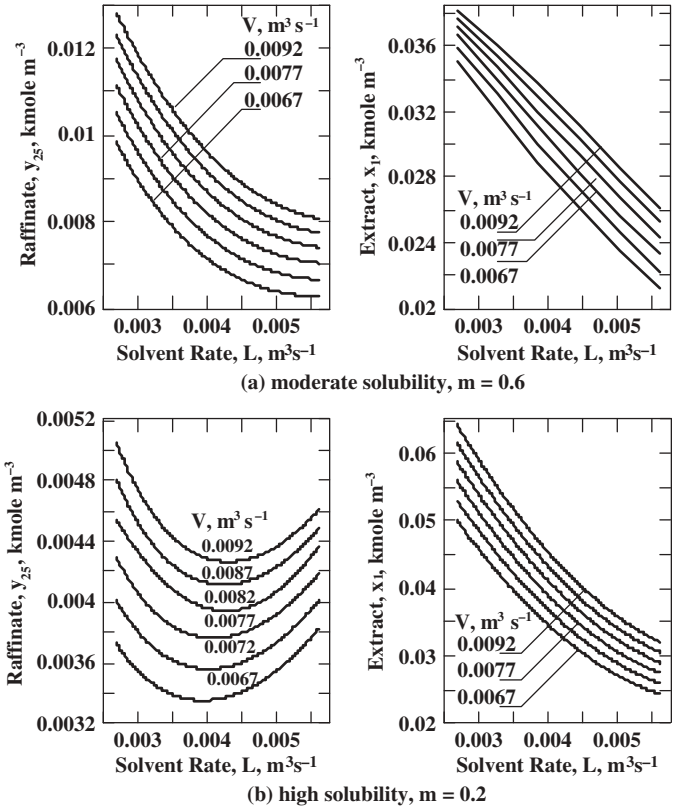

FIG. 7. Effect of phase flow rates on raffinate and extract phase compositions in physical extraction (k = 0). (a) m = 0.6 (b) m = 0.2.

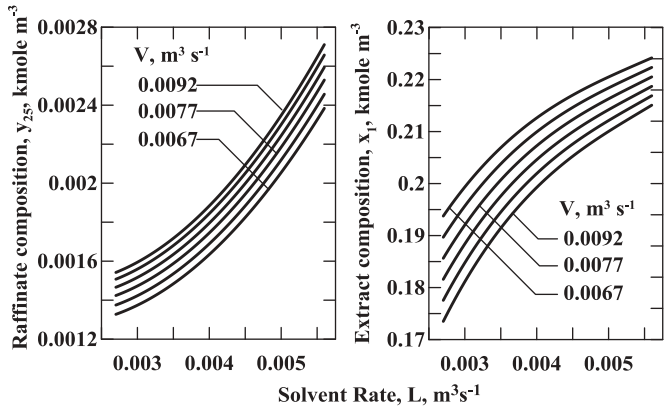

FIG. 8. Effect of phase flow rates on raffinate and extract phase compositions in the case of infinitely fast reaction.

flow rate in the various cases are not obvious and will be analyzed below.

Analysis of Raffinate Composition Trends

Figure 7a presents the case of a moderately soluble solute, m = 0.6. It shows that as the solvent rate increases

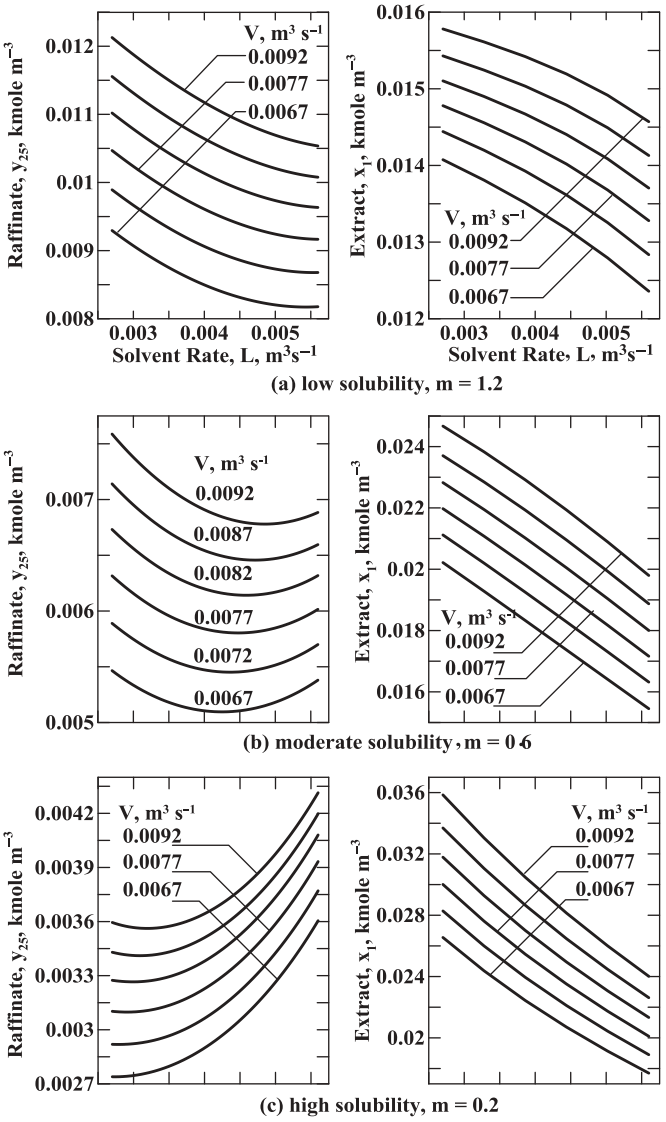

FIG. 9. Effect of phase flow rates in the case of a slow extract phase reaction, k = 0.0015 s^{-1} (a) m = 1.2, (b) m = 0.6, (c) m = 0.2.

the solute concentration in the raffinate product decreases. This trend is similar to that obtained when the effect of the flow rate on the mass transfer resistance is neglected (42) either by assuming theoretical stages or by lumping the mass transfer efficiency effect into a pseudo-equilibrium line.

In the case of physical extraction, the assumption of equilibrium implies that $K_A.a' \to \infty$, then $\beta \to \infty$, $\alpha \to 0$, and $c = g$, in this case Eq. (14) is reduced to a form obtainable from the classical Kremser equation (43).

$$\frac{y_N}{y_f} = 1 - \frac{(-1)(1-c^N)}{c^{N+1}-1} = \frac{g^{N+1}-g^N}{g^{N+1}-1} \tag{27}$$

$$\frac{d(y_N/y_f)}{dL} = \frac{d(y_N/y_f)}{dg} \times \frac{dg}{dL} \tag{28}$$

Differentiation of Eq. (27) gives

$$\frac{d(y_N/y_f)}{dg} = \frac{\sum_{i=0}^{N} i g^{-(i+1)}}{\left(\sum_{i=0}^{N} g^{-i}\right)^2} \tag{29}$$

which is always positive. On the other hand, $dg/dL = -mV/L^2$, is always negative, therefore $\frac{d(y_N/y_f)}{dL}$ given by Eq. (28) will be always negative regardless the value of m.

When the mass transfer resistance is not neglected, the above simplifying assumptions do not apply to Eq. (14), and the obtained trend depends on the value of m. Figure 7b shows that for the higher solute solubility case, m = 0.2 rather than 0.6, the raffinate composition increases rather than continuing to decrease at high flow rates, exhibiting a minimum at some intermediate flow rate.

For the limiting condition when $m = 0$, the separation factor $g = 0$, and $c = \alpha$. Also when $m = 0$, $K_A \to k_A$, $\beta \to \beta'$ and $\alpha \to \alpha'$. Eq. (14) may be thus simplified to

$$\frac{y_N}{y_f} = 1 - \frac{(\alpha'-1)\left(1-\alpha'^N\right)}{(\alpha'-1)} = \alpha'^N = e^{-N\beta'} \tag{30}$$

which is Eq. (19) derived for the infinitely fast reaction.

$$\frac{d(y_N/y_f)}{dL} = \frac{d(y_N/y_f)}{d\beta'} \times \frac{d\beta'}{dL} \tag{31}$$

Since h decreases as the continuous phase flow rate L increases, as explained in section (3), $d\beta'/dL$ is always negative. Also, $d(y_N/y_f)/d\beta' = -Ne^{-N\beta'}$ is always negative. Therefore, y_N/y_f increases with the increase of the solvent flow rate L as shown in Fig. 8, which depicts the trends obtained for a very fast reaction. An increase of the solvent rate results in an increase in raffinate concentration, that is, impairment of obtainable product purity. In such cases, increase in either the feed composition, or flow rate cannot be compensated by an increase in the solvent rate. The concentration of B in the extract phase follows the expected trend of increasing with the solvent rate and decreasing with the feed rate.

At the other limiting condition of infinite solvent to feed ratio, $V/L = 0$, then $g = 0$, $c = \alpha$, $\beta \to \infty$ and $\alpha \to 0$. Substituting $c = \alpha = 0$ in Eq. (14) gives $y_N/y_f = 0$ which means that the solute in the raffinate product is completely eliminated irrespective of the presence of a chemical reaction. The same result could be obtained from Eq. (27) which is based on neglecting the mass transfer resistance.

Effect of Solubility and Reaction Rate

Figure 9 reports the results of presence of a slow extract phase chemical reaction. The effect of a chemical reaction is similar to that of increased solubility. It is seen from Fig. 9a, that for a rate constant of (0.0015 s^{-1}), the raffinate concentration follows the expected trend of decreasing with increased solvent rate for low solute solubility ($m = 1.2$). It is characterized by a minimum in the case of moderate solubility ($m = 0.6$) as shown in Fig. 9b and it increases monotonically with the solvent rate for the high solubility case ($m = 0.2$) as shown in Fig. 9c.

The trend of variation of raffinate composition with changing flow rates arises from two opposing tendencies. The increase in either flow rate is associated with a negative effect on raffinate purity owing to decrease of the effective mass transfer contact height on a plate, while the increase in solvent rate has a positive effect because of the increased mass transfer driving force. In the cases of pure physical extraction or slow extract phase reaction, raffinate purity is improved with increasing solvent rate up to the limit where the reduction in mass transfer rate counter balances the effect of the increased driving force arising from dilution.

The solvent rate at which the hydrodynamic impairment of purity starts to prevail depends on the equilibrium solubility and the reaction rate. Since the increase of the above two factors is associated with an improvement in driving force, the flow rate at which purity starts to deteriorate is higher the higher the solubility or reaction rate or both. Considering the case of physical extraction, the solvent rate at which y_N/y_f is minimum may be obtained by differentiating Eq. (14) and setting $d(y_N/y_f)/dL = 0$. This gives

$$\frac{dc/dL}{d\alpha/dL} - \frac{(c^{N+1} - c^N)(c^N - 1)}{(\alpha - 1)(c^{2N} - (N+1)c^N + Nc^{N-1})} = 0 \qquad (32)$$

For given values of system physical properties, column dimensions, feed flow rate, and solubility (m), all of c, α, dc/dL, and $d\alpha/dL$ are functions of L alone. For $m = 0.2$, Eq. (32) is satisfied at intermediate values of L corresponding to the minima shown in Fig. 7b. For values of m, corresponding to relatively low or high solubility, Eq. (32) is not satisfied.

For the case of infinitely fast reactions or infinite solute solubility, no further improvement of the driving force is possible on increasing the solvent rate, it is already at its maximum because the solute concentration in the extract is zero. The raffinate purity therefore decreases monotonically with the increase of the solvent rate.

CONCLUSIONS

Steady state models have been developed for analyzing the performance of un-agitated perforated plate liquid-liquid extraction columns conducting an extract phase reaction. Three modes of interaction between mass transfer and chemical kinetics have been considered. These include the cases of physical extraction, slow extract phase reaction, and infinitely fast interfacial reaction. The derived models consider the effect of flow dynamics on the mass transfer taking place along the effective contact height on each plate. They are characterized by three dimensionless parameters α, g, and δ which reflect the column hydrodynamic behavior and transport properties of the handled liquids. Existing correlations relating phase flow rates to hydrodynamic and mass transfer performance variables of the system have been integrated into the computations of the model dimensionless parameters.

The effect of the reaction rate is illustrated by generating typical steady state composition profiles of the solute in the extract and raffinate phases and of the solvent phase reactant along a column in which an acid is removed from an aromatic hydrocarbon by an aqueous alkalized solvent. Different trends are observed for the distribution of the composition driving forces along the column in the studied cases.

In un-agitated perforated plate columns, the effect of changing flow rates on the obtained compositions of the final raffinate and extract products depends on the interaction between the kinetic regime, solute solubility, mass transfer conditions, and hydrodynamic performance of the system. Interesting trends have been observed for the effect of increasing the continuous solvent phase flow rate on the obtained raffinate purity for the studied cases. The trends have been analyzed in terms of the limiting conditions of infinite solubility and infinite solvent to feed ratio. They have been also compared with predictions of models based on neglecting the mass transfer fluid dynamic interactions in multi-stage separation cascades.

Increasing the continuous solvent flow rate in cases of limited solute solubility and slow reactions, results in improvement of the raffinate product purity. It is therefore possible in this case to keep the raffinate concentration despite feed composition disturbances by manipulation of the solvent rate. This is not the case for systems with high solute solubility and rather fast reactions where increasing the solvent rate is associated with deterioration of the final raffinate purity. In such cases feed composition disturbances would call for manipulation of the feed rate rather than the solvent rate.

NOMENCLATURE

a': interfacial area per unit volume of dispersed phase, $m^2\ m^{-3}$
$a_{1,2}$: $(b \pm \sqrt{b^2 - 4c})/2$
A_a: active plate area, m^2
b: $1 + \alpha + (1 - \alpha)\ g + \delta$
c: $(1 - \alpha)\ g + \alpha + \alpha\ \delta$
f: reaction stoichiometric coefficient
g: separation factor, $g = mV/L$

h: active contact height above a plate, $h = S\text{-}h_c$, m
h_c: depth of coalesced layer beneath a plate, m
K_A: overall mass transfer coefficient of reactant A, m s^{-1}
k: first order reaction rate constant, s^{-1}
k_A: mass transfer coefficient of reactant A in raffinate phase, m s^{-1}
k_B: mass transfer coefficient of reactant B in extract phase, m s^{-1}
L: volumetric flow rate of the continuous solvent phase, m^3 s^{-1}
m: slope of the equilibrium relation
n: plate number
N: total number of plates
S: tray spacing, m
V: dispersed phase feed flow rate, m^3 s^{-1}
x_B: reactant B concentration in continuous extract phase, kmol.m^{-3}
x_n: reactant A concentration in extract entering plate (n-1), kmol.m^{-3}
x_{Bn}: reactant B concentration in extract entering plate (n-1), kmol.m^{-3}
x_{BN+1}: reactant B concentration in the solvent feed phase, kmol.m^{-3}
y_n^*: raffinate composition in equilibrium with x_n, kmol.m^{-3}
y_f: reactant A concentration in the dispersed phase feed, kmol.m^{-3}
$\bar{y}_n$: mean dispersed phase reactant A concentration on plate n, kmol.m^{-3}
y_n: reactant A concentration in the dispersed phase entering plate (n+1), kmol.m^{-3}
z: elevation above tray level, m

Greek Symbols

α: dimensionless parameter, $\alpha = e^{-\beta}$
α': dimensionless parameter, $\alpha' = e^{-\beta'}$
β: dimensionless parameter, $\beta = K_A a' A_a \varphi h / V$
β': dimensionless parameter, $\beta' = k_A a' A_a \varphi h / V$
δ: dimensionless parameter, $\delta = (1-\varphi) A_a h k / L$
φ: dispersed phase holdup volume fraction

REFERENCES

1. Bart, H.-J.; Drumm, C.; Attarakih, M. M. (2008) Process intensification with reactive extraction columns. *Chem. Eng. Process*., 47 (5):745–754.
2. Bhave, R. R.; Sharm, M. M. (1983) Extraction of COS dissolved in n-heptane into aqueous sodium hydroxide: Phase transfer catalysis. *Chem. Eng. Sci*., 38 (1): 141–145.
3. Hlushak, S. P.; Simonin, J. P.; Caniffi, B.; Moisy, P.; Sorel, C.; Bernard, O. (2011) Description of partition equilibria for uranyl nitrate, nitric acid and water extracted by tributyl phosphate in dodecane. *Hydromet*., 109 (1–2): 97–105.
4. Jiang, J-Q.; Mwabonje, O. (2009) Phosphorus recovery by liquid–liquid extraction, *Sep. Sci. Technol*., 44 (13): 3258–3266.
5. Venkateswaran, P.; Palanivelu, K. (2004) Solvent extraction of hexavalent chromium with tetrabutyl ammonium bromide from aqueous solution. *Sep. Purif. Technol*., 40 (3): 279–284.
6. Chaturabul, S.; Wannachod, P; Rojanasiraprapa, B.; Summakasipong, S; Lothongkum, A. W.; Pancharoen, U. (2012) Arsenic removal from natural gas condensate using a pulsed sieve plate column and mass transfer efficiency. *Sep. Sci. Technol*., 47 (3):432–439
7. Kucka, L.; Richter, J.; Kenig, E. Y.; Górak, A. (2003) Determination of gas–liquid reaction kinetics with a stirred cell reactor. *Sep. Purif. Technol*., 31 (2):163–175.
8. Noeres, C.; Kenig, E. Y.; Górak, A. (2003) Modelling of reactive separation processes: reactive absorption and reactive distillation. *Chem. Eng. Process*., 42 (3):157–178.
9. Yung, K. K. L.; Smith, C. D.; Bowser, T. A.; Perera, J. M.; Stevens, G. W. (2012) The use of an ionic liquid in a Karr reciprocating plate extraction column: dispersed phase hold-up prediction. *Sep. Sci. Technol*., 47 (2): 346–353.
10. El-Rifai, M. A. (1975) Composition dynamics in multi-mixer-settler extractive reaction batteries. *Chem. Eng. Sci*., 30 (1): 79–87.
11. El-Rifai, M. A.; El Nashaie, S. S. E. H.; Kafafi, A. A. (1977) Analysis of a countercurrent tallow-splitting column. *Chem. Eng. Res. Des*., 55a: 59–63.
12. El Nashaie, S. S. E. H.; El-Rifai, M. A.; Abd El-Hakim, M. N. (1978) Effect of kinetic regime and axial dispersion on the dynamic response of counter flow extractive reactors. *Chem. Eng. Sci*., 33 (7): 847–852.
13. Mjalli, F. S.; Abdel-Jabbar, N. M.; Fletcher, J. P. (2005) Modeling, simulation and control of a scheibel liquid–liquid contactor: Part 1. Dynamic analysis and system identification. *Chem. Eng. Process*., 44 (5): 541–553.
14. Tang, X. J.; Luo, G. S.; Wang, J. D. (2005) An improved dynamic combined model for evaluating the mass transfer performances in extraction columns. *Chem. Eng. Sci*., 60 (16): 4409–4421.
15. Samani, M. G.; Safdari, J.; Asl, A. H.; Torab-Mostaedi, M. (2014) Effect of structural parameters on drop size distribution in pulsed packed columns. *Chem. Eng. Technol*., 37 (7): 1155–1162.
16. Schmidt, S. A.; Simon, M.; Attarakih, M. M.; Lagar, L.; Bart, H-J. (2006) Droplet population balance modeling, hydrodynamics and mass transfer. *Chem. Eng. Sci*., 61 (1): 246–256.
17. Liao, Y.; Lucas, D. (2010) A literature review on mechanisms and models for the coalescence process of fluid particles. *Chem. Eng. Sci*., 65 (10): 2851–2864.
18. Drumm, C.; Attarakih, M.; Hlawitschka, M. W.; Bart, H-J. (2010) One-group reduced population balance model for CFD simulation of a pilot-plant extraction column. *Ind. Eng. Chem. Res*., 49 (7): 3442–3451.
19. Jaradat, M.; Attarakih, M.; Bart, H-J. (2011) Advanced prediction of pulsed (packed and sieve plate) extraction columns performance using population balance modeling. *Chem. Eng. Res. Des*., 89 (12): 2752–2760.
20. Hlawitschkah, M. W.; Bart, H-J. (2012) CFD-mass transfer simulation of an RDC column. *Comput. Aided Chem. Eng*., 31: 920–924.
21. Attarakih, M.; Abu-Khader, M.; Bart, H-J. (2013) Modeling and dynamic analysis of a rotating disc contactor (RDC) extraction column using one primary and one secondary particle method (OPOSPM). *Chem. Eng. Sci*., 91 (22): 180–196.
22. Garner, F. H.; Ellis, S. R. M.; Hill, J. W. (1955) Perforated-plate extraction-column performance and wetting characteristics. *AIChE J*., 1 (2): 185–192.
23. Treybal, R. E. (1981) *Mass Transfer Operations*, 3rd ed.; McGraw Hill International Editions: Singapore.
24. Yadav, R. L.; Patwardhan, A. W. (2009) CFD modeling of sieve and pulsed-sieve plate extraction columns. *Chem. Eng. Res. Des*., 87 (1): 25–35.
25. Ettouney, R. S.; El-Rifai, M. A.; Ghallab, A. O. (2007) Steady state modeling of perforated plate extraction columns. *Chem. Eng. and Process*., 46 (8): 713–720.

26. Ettouney, R. S.; El-Rifai, M. A. (2011) Composition dynamics in perforated plate liquid extraction columns. *Chem. Eng. Res. Des*., 89 (11): 2228–2235.
27. Ettouney, R. S.; El-Rifai, M. A. (2012) Flow dynamics in perforated plate liquid extraction columns. *Chem. Eng. Res. Des*., 90 (10): 1417–1424.
28. Doraiswamy, L. K.; Sharma, M. M. (1984) *Heterogeneous Reactions: Analysis, Examples, and Reactor Design*, Vol. 2; Wiley-Interscience Publication: New York.
29. Levenspiel, O. (1999) *Chemical Reaction Engineering*, 3rd ed.; Wiley: New York.
30. Godfrey, J. C.; Slater, M. J. (1991) Slip velocity relationships for liquid-liquid extraction columns. *Chem. Eng. Res. Des*., 69a: 130–141.
31. Attarakih, M. M.; Bart, H-J.; Steinmetza, T.; Dietzena, M.; Faqir, N. M. (2008) LLECMOD: A bivariate population balance simulation tool for liquid-liquid extraction columns. *The Open Chemical Engineering Journal*, 2: 10–34.
32. Hayworth, C. B.; Treybal, R. E. (1950) Drop formation in two-liquid-phase systems. *Ind. Eng. Chem*., 42: 1174–1181.
33. Zenz, F. A. (1957) Calculate fluidization rates. *Pet. Refiner*, 36 (8):147–155.
34. Bussolari, R. S.; Schiff, S.; Treybal, R. E. (1953) Flow of liquids through perforated-plate liquid extraction towers. *Ind. Eng. Chem*., 45 (11):2413–2417.
35. Newman, A. B. (1931) The drying of porous solids: Diffusion and surface emission equations. *Trans.Am.Inst.Chem.Eng*., 27:203–220.
36. Kronig, R.; Brink, J. (1950) On the theory of extraction from falling droplets. *Appl. Sci. Res*., 2(1):142–154.
37. Handlos, A. E.; Baron, T. (1957) Mass and heat transfer from drops in liquid-liquid extraction. *AIChE J*., 3(1):127–135.
38. Garner, F. H.; Tayeban, M. (1960) The importance of the wake in mass transfer from both continuous and dispersed phase systems. *An. Real. Soc. Espan. Fis. Y. Quim*, 56-b:479–490.
39. Clift, R.; Grace, J. R.; Weber, M. E. (1978) *Bubbles*, *Drops and Particles*; Academic Press: New York.
40. Wilke, C. R.; Lee, C.Y. (1955) Estimation of diffusion coefficients for gases and vapors. *Ind. Eng. Chem*., 47:1253–1257.
41. Hayduk, W.; Minhas, B. S. (1982) Correlations for prediction of molecular diffusivities in liquids. *Can. J. Chem. Eng*., 60 (2):295–299.
42. Kremser, A. (1930). Theoretical analysis of absorption process. *Nat. Pet. News*, 22(21):48–52.
43. Turton, R.; Bailie, R. C.; Whiting, W. B.; Shaeiwitz, J. A. (2003) *Analysis, Synthesis, and Design of Chemical Processes*, 2nd ed.; Prentice Hall: New Jersey.